

Reconfigurable Intelligent Surface Aided Wireless Localization

Yiming Liu, Erwu Liu and Rui Wang

College of Electronics and Information Engineering, Tongji University, Shanghai, China

Emails: ymliu_970131@tongji.edu.cn, erwu.liu@ieee.org, ruiwang@tongji.edu.cn

Abstract—The advantages of millimeter-wave and large antenna arrays technologies for accurate wireless localization received extensive attentions recently. However, how to further improve the accuracy of wireless localization, even in the case of obstructed line-of-sight, is largely undiscovered. In this paper, the reconfigurable intelligent surface (RIS) is introduced into the system to make the positioning more accurate. First, we establish the three-dimensional RIS-assisted wireless localization channel model. After that, we derive the Fisher information matrix and the Cramer-Rao lower bound for evaluating the estimation of absolute mobile station position. Finally, we propose an alternative optimization method and a gradient decent method to optimize the reflect beamforming, which aims to minimize the Cramer-Rao lower bound to obtain a more accurate estimation. Our results show that the proposed methods significantly improve the accuracy of positioning, and decimeter-level or even centimeter-level positioning can be achieved by utilizing the RIS with a large number of reflecting elements.

Index Terms—Wireless localization, reconfigurable intelligent surface, millimeter-wave, Cramer-Rao lower bound, reflect beamforming design.

I. INTRODUCTION

The fifth generation (5G) wireless technology offers great opportunities for accurate wireless localization due to the very high carrier frequency and large antenna arrays. Moreover, the sixth generation (6G) systems continue to develop towards even higher frequency ranges, *e.g.*, at the millimeter-wave (mm-wave) as well as Tera Hertz (THz) ranges. The 6G white paper on localization and sensing released by University of Oulu [1] points out that 6G systems will not only provide ubiquitous communication but also empower high accuracy localization due to the very fine angular resolutions. Decimeter-level or even centimeter-level positioning will be achieved by taking advantages of the new 6G key technology enablers.

The advantages of mm-wave and large antenna arrays for accurate wireless localization have been extensively studied. Jeong, *et al.*, propose an active beamforming method to enhance the localization accuracy of distributed antenna systems [2]. Shahmansoori, *et al.*, study the position and orientation estimation through mm-wave massive multiple-input multiple-output (MIMO) systems [3]. Wang, Wu, and Shen prove the asymptotic spatial orthogonality of large-scale MIMO localization with general non-orthogonal waveforms [4]. They also derive the Fisher information matrices for the position and orientation to characterize the performance bounds of MIMO localization. Zhou, *et al.*, focus on active beamforming

to reduce the localization error, and propose a successive localization and beamforming scheme [5].

However, how to further improve the accuracy of wireless localization, even in the case of obstructed line-of-sight, is largely undiscovered. Thus, in this paper, we introduce the reconfigurable intelligent surface (RIS), which is an efficient method to control the wavefront of the impinging signals, into the system to make the positioning more accurate and energy efficient. Our prior work shows that an RIS-assisted wireless communication system can achieve both high spectral and energy efficiency [6]. Wu and Zhang verify that the RIS is able to drastically enhance the link quality over the conventional setup without the RIS [7].

In this paper, we introduce the RIS into the wireless localization system, and focus on the (passive) reflect beamforming to reduce the localization error. We first build the three-dimensional RIS-assisted wireless localization system model. After that, we derive the Fisher information matrix and the Cramer-Rao lower bound for the estimate of absolute mobile station (MS) position. For the sake of convenience in reflect beamforming design, we separate the response of RIS in the Fisher information matrix. Finally, we propose an alternative optimization method and a gradient decent method to optimize the reflect beamforming, which aims to minimize the Cramer-Rao lower bound. Our results show that the proposed methods significantly improve the accuracy of positioning, and decimeter-level or even centimeter-level positioning can be achieved by utilizing the RIS with a large number of reflecting elements.

II. SYSTEM AND CHANNEL MODEL

Encouraged by the potential of mm-wave signals and large antenna arrays to improve the accuracy of positioning, many standardized channel models have started to emerge [3], [5], [8]. We base the evaluation of our work on these models while introducing the RIS into the system to make the MS positioning more accurate. Introducing RIS can provide extra reflection paths which help in the estimation of MS position. On the one hand, it makes the positioning become possible when the line-of-sight is obstructed; On the other hand, it adds more position information for estimation.

A. System Model

We consider an RIS-assisted wireless localization system as illustrated in Fig. 1, where the base station (BS) is equipped

with N_t antennas, the MS is equipped with N_r antennas, and the RIS is equipped with N reflecting elements. The BS and MS are placed in the horizontal plane, along the y -axis direction, and the RIS is placed in the vertical plane. Although the BS and MS are equipped with a large number of antennas, they can fit within the compact form because of the small wavelength of mm-wave. Thus, they can be viewed as two points, and the positions of them are respectively denoted as $\mathbf{p} = [p_x, p_y, 0]^T$ and $\mathbf{q} = [q_x, q_y, 0]^T$. Compared with the BS and MS, the RIS has a much larger size, thus each reflecting element needs to be considered separately. The position of the i th reflecting element is denoted as $\mathbf{s}^i = [s_x^i, s_y^i, s_z^i]^T$. The values of \mathbf{p} and \mathbf{s}^i are assumed to be known, while the value of \mathbf{q} is unknown and requires to be estimated.

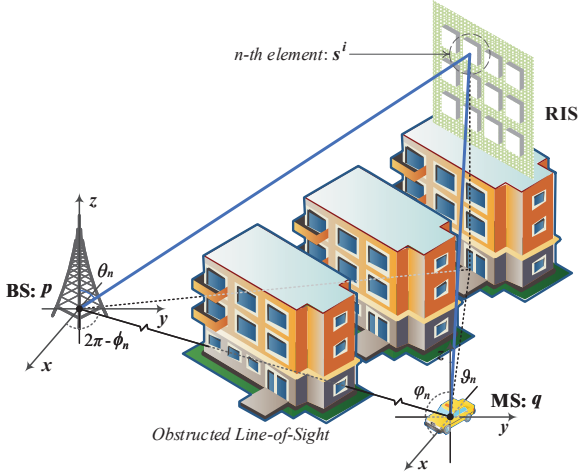


Fig. 1. The RIS-assisted wireless localization system with an N_t -antenna BS, an N_r -antenna MS, and an RIS comprising N reflecting elements. This paper considers the case that the line-of-sight is obstructed by some blockages.

In this paper, we focus on the case that the line-of-sight is obstructed, thus there exist N reflection paths through RIS. The elevation and azimuth angle-of-departure (AoD) of the i th path are denoted as θ_i and ϕ_i . The elevation and azimuth angle-of-arrival (AoA) of the i th path are denoted as ϑ_i and φ_i . Due to that the positions of BS and RIS are fixed and known, we can obtain the values of θ_i and ϕ_i by means of the geometrical relationship between them. The values of ϑ_i and φ_i are unknown and requires to be estimated. In addition, position estimate is equivalent with the azimuth and elevation AoA estimate due to the geometrical relationship.

B. Channel Model

We ignore the bounce reflections from the ground or other scatterers, since such paths get attenuated much more significantly than the paths through RIS. Based on the system model given above, the $N_r \times N_t$ channel matrix can be expressed as

$$\tilde{\mathbf{H}} = \mathbf{\Lambda}_r(\mathbf{H}\Phi)\mathbf{\Lambda}_t^H. \quad (1)$$

where the matrices $\mathbf{\Lambda}_t$ and $\mathbf{\Lambda}_r$ are the array response matrices at BS and MS, the diagonal matrix \mathbf{H} is the propagation gain

matrix of N paths, and the diagonal matrix Φ represents the operations at the RIS. The array response matrices $\mathbf{\Lambda}_t$ and $\mathbf{\Lambda}_r$ depend on the angular parameters, given by

$$\mathbf{\Lambda}_t = [\mathbf{a}_t(\theta_1, \phi_1), \dots, \mathbf{a}_t(\theta_N, \phi_N)] \in \mathbb{C}^{N_t \times N}, \quad (2)$$

$$\mathbf{\Lambda}_r = [\mathbf{a}_r(\vartheta_1, \varphi_1), \dots, \mathbf{a}_r(\vartheta_N, \varphi_N)] \in \mathbb{C}^{N_r \times N}, \quad (3)$$

where the i th column vectors $\mathbf{a}_t(\theta_i, \phi_i)$ and $\mathbf{a}_r(\vartheta_i, \varphi_i)$ are

$$\mathbf{a}_t(\theta_i, \phi_i) = [e^{j(1-k)\sin\theta_i\sin\phi_i}, \dots, e^{j(N_t-1)k\sin\theta_i\sin\phi_i}]^T, \quad (4)$$

$$\mathbf{a}_r(\vartheta_i, \varphi_i) = [e^{j(1-k)\sin\vartheta_i\sin\varphi_i}, \dots, e^{j(N_r-1)k\sin\vartheta_i\sin\varphi_i}]^T. \quad (5)$$

The parameter $k = 2\pi d/\lambda$ where d is the separation between transmit/receive antennas at BS/MS, and λ is the wavelength of transmitted signal. The diagonal matrix $\Phi = \text{diag}[e^{j\boldsymbol{\varrho}}]$ where $e^{j\boldsymbol{\varrho}}$ is an element-wise power operation, and the $N \times 1$ vector $\boldsymbol{\varrho} = [\varrho_1, \dots, \varrho_N]^T$ represents the phase shifts of N reflecting elements at RIS. The diagonal matrix $\mathbf{H} = \text{diag}[\mathbf{h}]$ where the $N \times 1$ vector $\mathbf{h} = [h_1, \dots, h_N]^T$ represents the propagation gains of N reflection paths, and the entries in it are independent and identically distributed.

C. Received Signal Model

The signal transmitted by the BS is denoted as $\mathbf{X} \in \mathbb{C}^{N_t \times L}$ where L represents the number of consumed time slots, and the column vector $\mathbf{x}(i)$ in it represents the signal transmitted at the i th time slot. Applying the vectorization operation, the received signal $\mathbf{y} \in \mathbb{C}^{L N_r \times 1}$ at the MS can be expressed as

$$\mathbf{y} = \begin{bmatrix} \mathbf{y}(1) \\ \mathbf{y}(2) \\ \vdots \\ \mathbf{y}(L) \end{bmatrix} = \begin{bmatrix} \tilde{\mathbf{H}}\mathbf{x}(1) \\ \tilde{\mathbf{H}}\mathbf{x}(2) \\ \vdots \\ \tilde{\mathbf{H}}\mathbf{x}(L) \end{bmatrix} + \begin{bmatrix} \mathbf{n} \\ \mathbf{n} \\ \vdots \\ \mathbf{n} \end{bmatrix}, \quad (6)$$

where the vector $\mathbf{n} \in \mathbb{C}^{N_r \times 1}$ is an additive white Gaussian noise with the elements independently drawn from $\mathcal{CN}(0, \sigma^2)$, and the transmit power at the l th slot is $p_{\text{BS}} = \mathbb{E}\{\mathbf{x}^H(l)\mathbf{x}(l)\}$.

III. CRAMER-RAO BOUND ON POSITION ESTIMATION

Based on the channel model, the unknown parameters to be estimated can be denoted as a $3N$ dimensional vector $\boldsymbol{\eta}$,

$$\boldsymbol{\eta} = [\vartheta_1, \dots, \vartheta_N, \varphi_1, \dots, \varphi_N, h_1, \dots, h_N]^T. \quad (7)$$

We denote the unbiased estimator of $\boldsymbol{\eta}$ as $\hat{\boldsymbol{\eta}}$, and based on the Cramer-Rao theorem [9], [10], the mean-square error is bounded as

$$\mathbb{E}[(\hat{\boldsymbol{\eta}} - \boldsymbol{\eta})(\hat{\boldsymbol{\eta}} - \boldsymbol{\eta})^H] \geq \mathbf{J}_{\boldsymbol{\eta}}^{-1}, \quad (8)$$

where $\mathbf{J}_{\boldsymbol{\eta}}$ is the $3N \times 3N$ Fisher information matrix, and $[\mathbf{J}_{\boldsymbol{\eta}}^{-1}]_{m,m}$ is the Cramer-Rao lower bound for the m th parameter estimate. The (m, n) th entry of $\mathbf{J}_{\boldsymbol{\eta}}$ is defined as

$$\begin{aligned} [\mathbf{J}_{\boldsymbol{\eta}}]_{m,n} &\triangleq \mathbb{E} \left[-\frac{\partial^2 \ln p(\mathbf{y}; \boldsymbol{\eta})}{\partial \eta_m \partial \eta_n} \right] \\ &\equiv \mathbb{E} \left[\frac{\partial \ln p(\mathbf{y}; \boldsymbol{\eta})}{\partial \eta_m} \frac{\partial \ln p(\mathbf{y}; \boldsymbol{\eta})}{\partial \eta_n} \right], \end{aligned} \quad (9)$$

where $p(\mathbf{y}; \boldsymbol{\eta})$ is the likelihood function of the random vector \mathbf{y} conditioned on $\boldsymbol{\eta}$, and η_m is the m th entry of $\boldsymbol{\eta}$. The proof of the identity in Eq. (9) is given in [10]. Based on the received signal model, $p(\mathbf{y}; \boldsymbol{\eta})$ can be written as

$$p(\mathbf{y}; \boldsymbol{\eta}) = (2\pi)^{-\frac{LN_r}{2}} (\det \sigma^2 \mathbf{I})^{-\frac{1}{2}} e^{-\frac{1}{2} [\boldsymbol{\mu}^H (\sigma^2 \mathbf{I})^{-1} \boldsymbol{\mu}]}, \quad (10)$$

where the vector $\boldsymbol{\mu}$ is the mean vector of the random vector \mathbf{y} conditioned on $\boldsymbol{\eta}$.

To further obtain the Fisher information matrix \mathbf{J}_η , we first present the following Lemma from Eq. (6) in [11]:

Lemma. For an N dimensional random vector \mathbf{y} which obeys the symmetric complex Gaussian distribution $\mathcal{CN}(\boldsymbol{\mu}, \boldsymbol{\Sigma})$, the (m, n) th entry of the Fisher information matrix is given by

$$[\mathbf{J}]_{m,n} = 2\Re \left\{ \frac{\partial \boldsymbol{\mu}^H}{\partial \eta_m} \boldsymbol{\Sigma}^{-1} \frac{\partial \boldsymbol{\mu}}{\partial \eta_n} \right\} + \Im \left\{ \boldsymbol{\Sigma}^{-1} \frac{\partial \boldsymbol{\Sigma}}{\partial \eta_m} \boldsymbol{\Sigma}^{-1} \frac{\partial \boldsymbol{\Sigma}}{\partial \eta_n} \right\}. \quad (11)$$

By using the above Lemma, the (m, n) th entry of \mathbf{J}_η in Eq. (9) can be rewritten as

$$[\mathbf{J}_\eta]_{m,n} = \sum_{l=1}^L \frac{2}{\sigma^2} \Re \left\{ \frac{\partial \boldsymbol{\mu}^H(l)}{\partial \eta_m} \frac{\partial \boldsymbol{\mu}(l)}{\partial \eta_n} \right\} = \sum_{l=1}^L [\mathbf{J}_\eta(l)]_{m,n}, \quad (12)$$

where the mean vector $\boldsymbol{\mu}(l) = \tilde{\mathbf{H}}\mathbf{x}(l)$. Eq. (12) demonstrates that the Fisher information matrix \mathbf{J}_η is the sum of the Fisher information matrix $\mathbf{J}_\eta(l)$ at each time slot. The rest in this section gives the solving process of $\mathbf{J}_\eta(l)$.

We rewrite the Fisher information matrix $\mathbf{J}_\eta(l)$ as a partitioned matrix in Eq. (13) which is for later use.

$$\mathbf{J}_\eta(l) = \frac{2}{\sigma^2} \left[\begin{array}{c|c} \mathcal{A} & \mathcal{B} \\ \hline \mathcal{C} & \mathcal{D} \end{array} \right] \left. \begin{array}{l} \left. \vphantom{\begin{array}{c|c} \mathcal{A} & \mathcal{B} \\ \hline \mathcal{C} & \mathcal{D} \end{array}} \right\} 2N \\ \left. \vphantom{\begin{array}{c|c} \mathcal{A} & \mathcal{B} \\ \hline \mathcal{C} & \mathcal{D} \end{array}} \right\} N \end{array} \right\} \quad (13)$$

where the entries in submatrix \mathcal{A} contain the partial derivatives with respect to the azimuth/elevation AoA, while the entries in submatrices \mathcal{B} , \mathcal{C} and \mathcal{D} contain the partial derivatives with respect to the propagation gains.

Next, we give the partial derivatives of $\boldsymbol{\mu}(l)$ with respect to the azimuth/elevation AoA. Before giving it, we first give the partial derivatives of the matrix $\boldsymbol{\Lambda}_r(\mathbf{H}\Phi)\boldsymbol{\Lambda}_t^H$. The (m, n) th entry of the matrix $\boldsymbol{\Lambda}_r(\mathbf{H}\Phi)\boldsymbol{\Lambda}_t^H$ is given by

$$[\boldsymbol{\Lambda}_r(\mathbf{H}\Phi)\boldsymbol{\Lambda}_t^H]_{m,n} = \sum_{i=1}^N h_i e^{j[\varrho_i + (m-1)\xi_i + (1-n)\zeta_i]}, \quad (14)$$

where $\xi_i = k \sin \vartheta_i \sin \varphi_i$ and $\zeta_i = k \sin \theta_i \sin \phi_i$. To separate the response of RIS, the partial derivatives of the matrix $\boldsymbol{\Lambda}_r(\mathbf{H}\Phi)\boldsymbol{\Lambda}_t^H$ with respect to the azimuth/elevation AoA are given by

$$\frac{\partial [\boldsymbol{\Lambda}_r(\mathbf{H}\Phi)\boldsymbol{\Lambda}_t^H]}{\partial \vartheta_i} = e^{j\varrho_i} \dot{\boldsymbol{\Xi}}_i \in \mathbb{C}^{N_r \times N_t}, \quad (15)$$

$$\frac{\partial [\boldsymbol{\Lambda}_r(\mathbf{H}\Phi)\boldsymbol{\Lambda}_t^H]}{\partial \varphi_i} = e^{j\varrho_i} \ddot{\boldsymbol{\Xi}}_i \in \mathbb{C}^{N_r \times N_t}, \quad (16)$$

where

$$[\dot{\boldsymbol{\Xi}}_i]_{m,n} = h_i j(m-1)k \sin \varphi_i \cos \vartheta_i e^{j[(m-1)\xi_i + (1-n)\zeta_i]}, \quad (17)$$

$$[\ddot{\boldsymbol{\Xi}}_i]_{m,n} = h_i j(m-1)k \sin \vartheta_i \cos \varphi_i e^{j[(m-1)\xi_i + (1-n)\zeta_i]}. \quad (18)$$

Then, we obtain the partial derivatives of $\boldsymbol{\mu}(l)$ with respect to the azimuth/elevation AoA as follows:

$$\frac{\partial \boldsymbol{\mu}(l)}{\partial \vartheta_i} = e^{j\varrho_i} \dot{\boldsymbol{\omega}}_i(l) \in \mathbb{C}^{N_r \times 1}, \quad (19)$$

$$\frac{\partial \boldsymbol{\mu}(l)}{\partial \varphi_i} = e^{j\varrho_i} \ddot{\boldsymbol{\omega}}_i(l) \in \mathbb{C}^{N_r \times 1}, \quad (20)$$

where $\dot{\boldsymbol{\omega}}_i(l) = \dot{\boldsymbol{\Xi}}_i \mathbf{x}(l)$ and $\ddot{\boldsymbol{\omega}}_i(l) = \ddot{\boldsymbol{\Xi}}_i \mathbf{x}(l)$.

Compared with the azimuth/elevation AoA, what we are more interested in is the absolute MS position $\mathbf{q}_{1:2} = [q_x, q_y]^T$. The Fisher information matrix of it can be obtained by means of the $2 \times 3N$ transformation matrix \mathbf{T} , which is expressed as

$$\mathbf{J}_q(l) = \mathbf{T} \mathbf{J}_\eta(l) \mathbf{T}^T, \quad (21)$$

where the transformation matrix \mathbf{T} is defined as

$$\mathbf{T} \triangleq \frac{\partial \boldsymbol{\eta}^T}{\partial \mathbf{q}_{1:2}}. \quad (22)$$

The entries of the transformation matrix \mathbf{T} can be obtained by the geometrical relationship between the azimuth/elevation AoA and the MS position which is shown as follows:

$$\vartheta_i = \arctan \left[\frac{\|\mathbf{q}_{1:2} - \mathbf{s}_{1:2}^i\|_2}{s_z^i} \right], \quad (23)$$

$$\varphi_i = \arccos \left[-\frac{|q_x - s_x^i|}{\|\mathbf{q}_{1:2} - \mathbf{s}_{1:2}^i\|_2} \right]. \quad (24)$$

Then, by computing the partial derivatives of the azimuth and elevation AoA with respect to the MS position, we obtain the transformation matrix \mathbf{T} as follows:

$$\mathbf{T} = \left[\underbrace{\boldsymbol{\mathcal{E}}}_N \quad \underbrace{\boldsymbol{\mathcal{F}}}_N \quad \underbrace{\boldsymbol{\mathcal{G}}}_N \right] \quad (25)$$

where the i th column vector of the submatrices $\boldsymbol{\mathcal{E}}$, $\boldsymbol{\mathcal{F}}$ and $\boldsymbol{\mathcal{G}}$ respectively are

$$[\boldsymbol{\mathcal{E}}]_i = \frac{\partial \vartheta_i}{\partial \mathbf{q}_{1:2}} = \frac{s_z^i}{\|\mathbf{q}_{1:2} - \mathbf{s}_{1:2}^i\|_2^2 + (s_z^i)^2} [-\cos \varphi_i, \sin \varphi_i]^T, \quad (26)$$

$$[\boldsymbol{\mathcal{F}}]_i = \frac{\partial \varphi_i}{\partial \mathbf{q}_{1:2}} = \frac{1}{\|\mathbf{q}_{1:2} - \mathbf{s}_{1:2}^i\|_2} [\sin \varphi_i, \cos \varphi_i]^T, \quad (27)$$

$$[\boldsymbol{\mathcal{G}}]_i = \frac{\partial h_i}{\partial \mathbf{q}_{1:2}} = [0, 0]^T. \quad (28)$$

The Eqs. (26) - (28) are derived in subsection A of Appendix. Because the $2 \times N$ submatrix $\boldsymbol{\mathcal{G}}$ is a zero matrix, then based on the multiplication principle of partitioned matrix, Eq. (21)

can be simplified as

$$\mathbf{J}_q(l) = \frac{2}{\sigma^2} \tilde{\mathbf{T}} \mathbf{A} \tilde{\mathbf{T}}^T, \quad (29)$$

where the matrix $\tilde{\mathbf{T}}$ consists of the submatrices \mathcal{E} and \mathcal{F} , and the matrix \mathbf{A} is the $2N \times 2N$ submatrix in Eq. (13).

We rewrite the matrix \mathbf{A} as a partitioned matrix as follows:

$$\mathbf{A} = \left[\begin{array}{c|c} \mathcal{H} & \mathcal{I} \\ \hline \mathcal{J} & \mathcal{K} \end{array} \right] \left. \begin{array}{l} \\ \\ \\ \\ \end{array} \right\} \begin{array}{l} N \\ N \\ N \\ N \end{array} \quad (30)$$

Based on the definition of the (m, n) th entry of $\mathbf{J}_q(l)$ in Eq. (12) and the partial derivatives of $\boldsymbol{\mu}(l)$ with respect to the azimuth/elevation AoA in Eqs. (19) and (20), we find that the response of RIS in the (m, n) th entry of the submatrix \mathcal{H} is same with those in the submatrices \mathcal{I} , \mathcal{J} and \mathcal{K} , which is $e^{j(\varrho_n - \varrho_m)}$. Then, the entries in the 2×2 Fisher information matrix $\mathbf{J}_q(l)$ can be given as

$$[\mathbf{J}_q(l)]_{1,1} = \frac{2}{\sigma^2} \sum_{m=1}^N \sum_{n=1}^N \Re \left[e^{j(\varrho_n - \varrho_m)} \kappa_{m,n}^{1,1}(l) \right], \quad (31)$$

$$[\mathbf{J}_q(l)]_{1,2} = \frac{2}{\sigma^2} \sum_{m=1}^N \sum_{n=1}^N \Re \left[e^{j(\varrho_n - \varrho_m)} \kappa_{m,n}^{1,2}(l) \right], \quad (32)$$

$$[\mathbf{J}_q(l)]_{2,1} = \frac{2}{\sigma^2} \sum_{m=1}^N \sum_{n=1}^N \Re \left[e^{j(\varrho_n - \varrho_m)} \kappa_{m,n}^{2,1}(l) \right], \quad (33)$$

$$[\mathbf{J}_q(l)]_{2,2} = \frac{2}{\sigma^2} \sum_{m=1}^N \sum_{n=1}^N \Re \left[e^{j(\varrho_n - \varrho_m)} \kappa_{m,n}^{2,2}(l) \right], \quad (34)$$

where the scalars $\kappa_{m,n}^{1,1}(l)$, $\kappa_{m,n}^{1,2}(l)$, $\kappa_{m,n}^{2,1}(l)$ and $\kappa_{m,n}^{2,2}(l)$ are

$$\begin{aligned} \kappa_{m,n}^{1,1}(l) &= \alpha_m^x \alpha_n^x \dot{\mathbf{c}}_m^H(l) \dot{\mathbf{c}}_n(l) + \beta_m^x \alpha_n^x \ddot{\mathbf{c}}_m^H(l) \dot{\mathbf{c}}_n(l) \\ &+ \alpha_m^x \beta_n^x \dot{\mathbf{c}}_m^H(l) \ddot{\mathbf{c}}_n(l) + \beta_m^x \beta_n^x \ddot{\mathbf{c}}_m^H(l) \ddot{\mathbf{c}}_n(l), \end{aligned} \quad (35)$$

$$\begin{aligned} \kappa_{m,n}^{1,2}(l) &= \alpha_m^x \alpha_n^y \dot{\mathbf{c}}_m^H(l) \dot{\mathbf{c}}_n(l) + \beta_m^x \alpha_n^y \ddot{\mathbf{c}}_m^H(l) \dot{\mathbf{c}}_n(l) \\ &+ \alpha_m^x \beta_n^y \dot{\mathbf{c}}_m^H(l) \ddot{\mathbf{c}}_n(l) + \beta_m^x \beta_n^y \ddot{\mathbf{c}}_m^H(l) \ddot{\mathbf{c}}_n(l), \end{aligned} \quad (36)$$

$$\begin{aligned} \kappa_{m,n}^{2,1}(l) &= \alpha_m^y \alpha_n^x \dot{\mathbf{c}}_m^H(l) \dot{\mathbf{c}}_n(l) + \beta_m^y \alpha_n^x \ddot{\mathbf{c}}_m^H(l) \dot{\mathbf{c}}_n(l) \\ &+ \alpha_m^y \beta_n^x \dot{\mathbf{c}}_m^H(l) \ddot{\mathbf{c}}_n(l) + \beta_m^y \beta_n^x \ddot{\mathbf{c}}_m^H(l) \ddot{\mathbf{c}}_n(l), \end{aligned} \quad (37)$$

$$\begin{aligned} \kappa_{m,n}^{2,2}(l) &= \alpha_m^y \alpha_n^y \dot{\mathbf{c}}_m^H(l) \dot{\mathbf{c}}_n(l) + \beta_m^y \alpha_n^y \ddot{\mathbf{c}}_m^H(l) \dot{\mathbf{c}}_n(l) \\ &+ \alpha_m^y \beta_n^y \dot{\mathbf{c}}_m^H(l) \ddot{\mathbf{c}}_n(l) + \beta_m^y \beta_n^y \ddot{\mathbf{c}}_m^H(l) \ddot{\mathbf{c}}_n(l), \end{aligned} \quad (38)$$

and the parameters α_m^x , α_m^y , β_m^x and β_m^y respectively are the first and second entries of $[\mathcal{E}]_m$ and $[\mathcal{F}]_m$. Then, by using Eq. (12), we obtain the entries of the Fisher information matrix \mathbf{J}_q as follows:

$$[\mathbf{J}_q]_{a,b} = \sum_{l=1}^L [\mathbf{J}_q(l)]_{a,b}, \quad a = 1, 2; \quad b = 1, 2. \quad (39)$$

Finally, we obtain the Cramer-Rao lower bound for the MS position estimate which is the trace of the inverse matrix of the Fisher information matrix \mathbf{J}_q . The above result can be summarized as a theorem:

Theorem. For an RIS-assisted wireless localization system modeled as Section II, the Cramer-Rao lower bound for the estimate of absolute MS position can be expressed as

$$CRLB = \mathfrak{Tr}(\mathbf{J}_q^{-1}) = \frac{[\mathbf{J}_q]_{1,1} + [\mathbf{J}_q]_{2,2}}{[\mathbf{J}_q]_{1,1} [\mathbf{J}_q]_{2,2} - [\mathbf{J}_q]_{1,2} [\mathbf{J}_q]_{2,1}}. \quad (40)$$

IV. REFLECT BEAMFORMING DESIGN AT RIS

In this paper, we aim to minimize the Cramer-Rao lower bound for the MS position estimate by optimizing the reflect beamforming at the RIS. Accordingly, the optimization problem can be formulated as

$$\begin{aligned} \min_{\boldsymbol{\varrho}} \quad & f(\boldsymbol{\varrho}) = \frac{[\mathbf{J}_q]_{1,1} + [\mathbf{J}_q]_{2,2}}{[\mathbf{J}_q]_{1,1} [\mathbf{J}_q]_{2,2} - [\mathbf{J}_q]_{1,2} [\mathbf{J}_q]_{2,1}} \\ \text{s. t.} \quad & 0 \leq \varrho_n \leq 2\pi, \quad \forall n = 1, \dots, N. \end{aligned} \quad (41)$$

Because the objective function in Eq. (41) is a non-convex fractional function, it is difficult to obtain the global optimal solution. To further analyze this problem, we utilize the *gradient decent method* (GDM) to make the reflect beamforming design. In the *gradient flow direction* which is defined as the direction of the negative gradient $-\nabla_{\boldsymbol{\varrho}} f(\boldsymbol{\varrho})$, the function $f(\boldsymbol{\varrho})$ decreases at the maximum descent rate. And each component of the gradient vector gives the rate of change of the scalar function in the component direction [12].

The function $f(\boldsymbol{\varrho})$ is a scalar function with respect to an $N \times 1$ vector-variable. Thus, the gradient of it is expressed as

$$\nabla_{\boldsymbol{\varrho}} f(\boldsymbol{\varrho}) = \left[\frac{\partial f(\boldsymbol{\varrho})}{\partial \varrho_1}, \frac{\partial f(\boldsymbol{\varrho})}{\partial \varrho_2}, \dots, \frac{\partial f(\boldsymbol{\varrho})}{\partial \varrho_N} \right]^T, \quad (42)$$

where the partial derivative of $f(\boldsymbol{\varrho})$ with respect to ϱ_i is given in Eq. (43) at the top of the next page. The parameters \mathfrak{N} and \mathfrak{D} in it represent the numerator and denominator of $f(\boldsymbol{\varrho})$, respectively, and the partial derivatives of the entries in the Fisher information matrix \mathbf{J}_q with respect to ϱ_i is given as follows:

$$\frac{\partial [\mathbf{J}_q]_{1,1}}{\partial \varrho_i} = \frac{4}{\sigma^2} \sum_{l=1}^L \sum_{n \neq i}^N \Re \left[j e^{j(\varrho_i - \varrho_n)} \kappa_{n,i}^{1,1}(l) \right], \quad (44)$$

$$\frac{\partial [\mathbf{J}_q]_{1,2}}{\partial \varrho_i} = \frac{4}{\sigma^2} \sum_{l=1}^L \sum_{n \neq i}^N \Re \left[j e^{j(\varrho_i - \varrho_n)} \kappa_{n,i}^{1,2}(l) \right], \quad (45)$$

$$\frac{\partial [\mathbf{J}_q]_{2,1}}{\partial \varrho_i} = \frac{4}{\sigma^2} \sum_{l=1}^L \sum_{n \neq i}^N \Re \left[j e^{j(\varrho_i - \varrho_n)} \kappa_{n,i}^{2,1}(l) \right], \quad (46)$$

$$\frac{\partial [\mathbf{J}_q]_{2,2}}{\partial \varrho_i} = \frac{4}{\sigma^2} \sum_{l=1}^L \sum_{n \neq i}^N \Re \left[j e^{j(\varrho_i - \varrho_n)} \kappa_{n,i}^{2,2}(l) \right]. \quad (47)$$

The Eqs. (44) - (47) are derived in subsection B of Appendix.

$$\frac{\partial f(\boldsymbol{\varrho})}{\partial \varrho_i} = \frac{\left(\frac{\partial [\mathbf{J}_q]_{1,1}}{\partial \varrho_i} + \frac{\partial [\mathbf{J}_q]_{2,2}}{\partial \varrho_i} \right) \mathfrak{D}\boldsymbol{\epsilon} - \mathfrak{N}_u \left(\frac{\partial [\mathbf{J}_q]_{1,1}}{\partial \varrho_i} [\mathbf{J}_q]_{2,2} + [\mathbf{J}_q]_{1,1} \frac{\partial [\mathbf{J}_q]_{2,2}}{\partial \varrho_i} - \frac{\partial [\mathbf{J}_q]_{1,2}}{\partial \varrho_i} [\mathbf{J}_q]_{2,1} - [\mathbf{J}_q]_{1,2} \frac{\partial [\mathbf{J}_q]_{2,1}}{\partial \varrho_i} \right)}{\mathfrak{D}\boldsymbol{\epsilon}^2} \quad (43)$$

It should be noted that the objective function $f(\boldsymbol{\varrho})$, *i.e.*, the Cramer-Rao lower bound for the MS position estimate is depend on the unknown parameter $\boldsymbol{\eta}$, and we cannot directly utilize the GDM to optimize the objective function. To address this challenge, we adopt *alternative optimization*, as illustrated in Algorithm 1. More specifically, we start at an initial phase shift vector, and alternately update the estimator of $\boldsymbol{\eta}$ and optimize the phase shift vector $\boldsymbol{\varrho}$, until they converge. The estimation method used in Algorithm 1 is provided in the journal version, and will not be discussed here due to space limitation, and the detailed step of GDM-based reflect beamforming design is illustrated in Algorithm 2.

Algorithm 1 The Proposed Alternative Optimization Method

- 1: Cramer-Rao lower bound: $f(\boldsymbol{\varrho})$.
 - 2: Initialize the phase shift vector $\boldsymbol{\varrho}[0]$.
 - 3: **while** $\hat{\boldsymbol{\eta}}$ and $\boldsymbol{\varrho}$ not converge **do**
 - 4: i^{th} iteration:
 - 5: Estimate the parameter vector $\boldsymbol{\eta}$ and denote as $\hat{\boldsymbol{\eta}}[i]$.
 - 6: Based on the current iteration estimator $\hat{\boldsymbol{\eta}}[i]$, the phase shift vector is optimized by using the GDM and denote as $\boldsymbol{\varrho}[i]$. The GDM used is illustrated in *Algorithm 2*.
 - 7: **end while**
 - 8: **Output:** The estimator $\hat{\boldsymbol{\eta}}$ and the reflect beamforming $\boldsymbol{\varrho}$.
-

Algorithm 2 The Proposed GDM-Based Reflect Beamforming

- 1: Objective Function: $f(\boldsymbol{\varrho}) = \mathfrak{T}\tau(\mathbf{J}_q^{-1})$.
 - 2: **Input:** The estimator $\hat{\boldsymbol{\eta}}[i]$.
 - 3: Set the number of iterations $j = 0$.
 - 4: Set the stop criterion for the loop: tolerance $\epsilon > 0$.
 - 5: Take the phase shift vector result of the previous iteration as the initialized phase shift vector $\boldsymbol{\varrho}[i] = \boldsymbol{\varrho}[i - 1]$.
 - 6: Compute the objective function value under current $\boldsymbol{\varrho}[i]$.
 - 7: **while** stop criterion $\Delta f(\boldsymbol{\varrho}[i]) > \epsilon$ is not satisfied **do**
 - 8: Update the number of iterations $j = j + 1$.
 - 9: Choose $-\nabla_{\boldsymbol{\varrho}} f(\boldsymbol{\varrho}[i])$ as the search direction.
 - 10: Choose the step size t via backtracking line search.
 - 11: Update the variable $\boldsymbol{\varrho}[i] := \boldsymbol{\varrho}[i] - t \nabla_{\boldsymbol{\varrho}} f(\boldsymbol{\varrho}[i])$.
 - 12: Compute the objective function difference $\Delta f(\boldsymbol{\varrho}[i])$.
 - 13: **end while**
 - 14: **Output:** j , sub-optimal reflect beamforming $\boldsymbol{\varrho}[i]$.
-

V. NUMERICAL RESULTS

This paper focuses on the impact of reflect beamforming on the Cramer-Rao lower bound for the MS position estimate,

and aims to minimize it¹. The estimation method is provided in the journal version, and will not be discussed here due to space limitation. Thus, we set up the system parameters to be known or have been estimated: the wavelength of mm-wave signal is set up as 0.006, $\mathbf{p} = [0, 0, 0]^T$, $\mathbf{q} = [50, 100, 0]^T$, and the RIS is a uniform planar array in the vertical plane where $\mathbf{s}^1 = [-20, 50, 20]^T$ and the separation between each reflecting element is 0.1, all in meters. The propagation gains h_i ($i = 1, \dots, N$) of N reflection paths are set up as random complex numbers which obey the distribution of $\mathcal{CN}(0, 1)$.

A. GDM-Based Reflect Beamforming

We first show the *convergence behaviour* of the proposed GDM-based algorithm in Fig. 2. In this simulation, we only consider 1 time slot consumed to transmit the pilot signal. The transmit and receive antenna numbers are both set up as 10, and the separation equals to half-wavelength 0.003. The RIS is set up as a 5×5 uniform planar array, *i.e.*, there exist 25 reflection paths. The SNR which is defined as $p_{BS}/(N_T \sigma^2)$ are set up as 30 dB and 40 dB. (The impact of *time slot number*, *reflecting element number*, and *SNR* on the Cramer-Rao lower bound will be discussed in the next subsection.) The initial phase shift vector is generated randomly with the elements independently drawn from the uniform distribution on $[0, 2\pi]$.

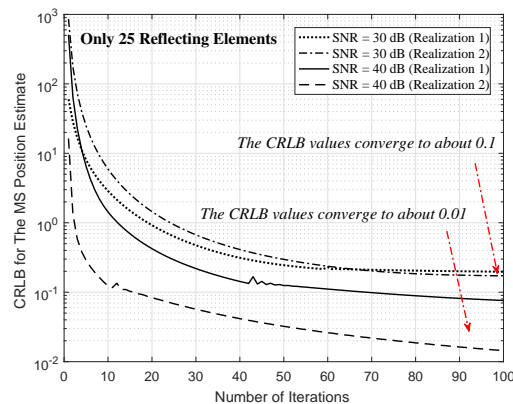


Fig. 2. The convergence behaviour of the proposed GDM-based algorithm.

The different dotted and solid curves in Fig. 2 are the gradient descent curves with different realizations of propagation gains. It is observed that by searching in the gradient flow direction, the Cramer-Rao lower bound values decrease quickly with the number of iterations. Compared with the

¹ Some prior works, like [3], [13], only provide the values of the Cramer-Rao lower bound for the estimate of AoA/AoD. But a small deviation in angle can result in a large deviation in absolute position, and the positioning accuracy can not be reflected directly. Thus, in this section, we present the values of the Cramer-Rao lower bound for the estimate of absolute MS position.

case without optimizing the reflect beamforming, there is a significant improvement on Cramer-Rao lower bound when using the proposed algorithm. In addition, the convergence results show that by optimizing the reflect beamforming, the Cramer-Rao lower bound for the estimate of absolute MS position can attain about 0.1 and 0.01, *i.e.*, decimeter-level or even centimeter-level positioning can be achieved by utilizing and optimizing the RIS, which satisfies the requirements of 6G wireless network technology.

B. Impact of Time Slot, Reflecting Element Number, and SNR

Next, we show the impact of time slot number, reflecting element number, and SNR in Fig. 3. In this experiment, we consider the consumed time slot number in the interval of [1, 10], the reflecting element number in the set of {16, 25, 36}, and the SNR in the set of {20, 30, 40} [dB]. It is observed that the Cramer-Rao lower bound decreases with the time slot number, the reflecting element number, and the SNR. The decimeter-level or even centimeter-level positioning can be achieved by utilizing the RIS with a large number of reflecting elements. But, it should be noted that the use of a large number of reflecting elements will result in the difficulty of estimating which is also the problem to be solved in the future.

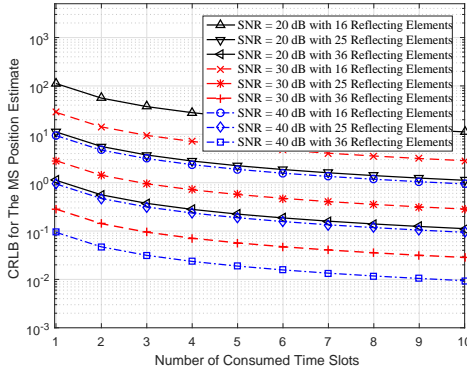


Fig. 3. Cramer-Rao lower bound for the MS position estimate versus time slot with different reflecting element numbers and SNRs.

C. Impact of MS Position

Finally, we show the impact of different MS position on the Cramer-Rao lower bound in Fig. 4. We consider two cases: one is that the x -coordinate of MS position is in the interval of [0, 100]; Another is that the y -coordinate of MS position is in the interval of [50, 150]. From the figure, we observe that the Cramer-Rao lower bound increases as the MS moves away from the RIS. More accurate localization can be achieved when the MS is closer to the RIS and more reflecting elements are utilized.

VI. CONCLUSION

In this paper, we utilize the advantages of mm-wave signals and large antenna arrays technologies, and introduce the RIS into the system to make the MS positioning more accurate. Our first contribution is to build the three-dimensional RIS-assisted wireless localization system model. After that, we

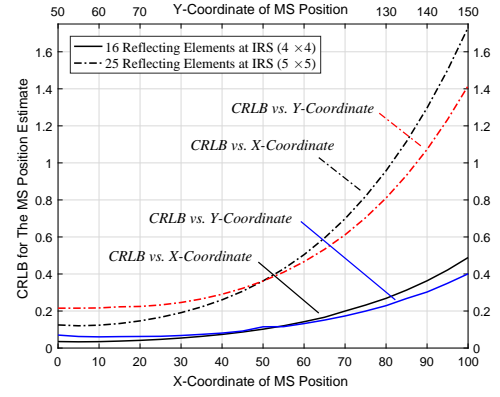


Fig. 4. Cramer-Rao lower bound for the MS position estimate versus x and y -coordinates of MS position with different numbers of reflecting elements.

derive the Fisher information matrix and the Cramer-Rao lower bound for the estimate of absolute MS position. Finally, we propose an alternative optimization method and a GDM-based algorithm to make the reflect beamforming design which aims to minimize the Cramer-Rao lower bound. The simulation results show that introducing RIS can make the positioning become possible when the line-of-sight is obstructed, and the proposed algorithm can make the estimation of MS position more accurate. The decimeter-level or even centimeter-level positioning can be achieved by utilizing the RIS with a large number of reflecting elements.

APPENDIX

A. Proof of Eqs. (26), (27) and (28)

By utilizing the geometrical relationship between the azimuth/elevation AoA and the MS position in Eqs. (24) and (23), and the derivatives of the inverse functions in Eq. (48),

$$(\arccos x)' = -\frac{1}{\sqrt{1-x^2}}, \quad (\arctan x)' = \frac{1}{1+x^2}, \quad (48)$$

we give the derivatives of ϑ_i and φ_i with respect to q_x as follows:

$$\begin{aligned} \frac{\partial \varphi_i}{\partial q_x} &= \frac{\partial \arccos \left[\frac{s_x^i - q_x}{\|\mathbf{q}_{1:2} - \mathbf{s}_{1:2}^i\|_2} \right]}{\partial q_x} \\ &= \frac{\| \mathbf{q}_{1:2} - \mathbf{s}_{1:2}^i \|_2 + (s_x^i - q_x) \frac{1}{2} \frac{1}{\| \mathbf{q}_{1:2} - \mathbf{s}_{1:2}^i \|_2} 2 (q_x - s_x^i)}{\sqrt{1 - \frac{(s_x^i - q_x)^2}{\| \mathbf{q}_{1:2} - \mathbf{s}_{1:2}^i \|_2^2}} \| \mathbf{q}_{1:2} - \mathbf{s}_{1:2}^i \|_2^2} \\ &= \frac{\| \mathbf{q}_{1:2} - \mathbf{s}_{1:2}^i \|_2 \left(1 - \frac{(s_x^i - q_x)^2}{\| \mathbf{q}_{1:2} - \mathbf{s}_{1:2}^i \|_2^2} \right)}{\sqrt{1 - \frac{(s_x^i - q_x)^2}{\| \mathbf{q}_{1:2} - \mathbf{s}_{1:2}^i \|_2^2}} \| \mathbf{q}_{1:2} - \mathbf{s}_{1:2}^i \|_2^2} \\ &= \frac{\sqrt{1 - \frac{(s_x^i - q_x)^2}{\| \mathbf{q}_{1:2} - \mathbf{s}_{1:2}^i \|_2^2}}}{\| \mathbf{q}_{1:2} - \mathbf{s}_{1:2}^i \|_2} = \frac{\sin \varphi_i}{\| \mathbf{q}_{1:2} - \mathbf{s}_{1:2}^i \|_2}, \end{aligned} \quad (49)$$

$$\begin{aligned}
\frac{\partial \vartheta_i}{\partial q_x} &= \frac{\partial \arctan \left[\frac{\|\mathbf{q}_{1:2} - \mathbf{s}_{1:2}^i\|_2}{s_z^i} \right]}{\partial q_x} \\
&= \frac{1}{1 + \frac{\|\mathbf{q}_{1:2} - \mathbf{s}_{1:2}^i\|_2^2}{(s_z^i)^2}} \cdot \frac{\frac{1}{\|\mathbf{q}_{1:2} - \mathbf{s}_{1:2}^i\|_2} \cdot 2 (q_x - s_x^i) s_z^i}{(s_z^i)^2} \\
&= \frac{1}{\|\mathbf{q}_{1:2} - \mathbf{s}_{1:2}^i\|_2^2 + (s_z^i)^2} \cdot \frac{(q_x - s_x^i) s_z^i}{\|\mathbf{q}_{1:2} - \mathbf{s}_{1:2}^i\|_2} \\
&= \frac{-s_z^i \cos \varphi_i}{\|\mathbf{q}_{1:2} - \mathbf{s}_{1:2}^i\|_2^2 + (s_z^i)^2}. \tag{50}
\end{aligned}$$

Similarly, we obtain the derivatives of ϑ_i and φ_i with respect to q_y as follows:

$$\frac{\partial \varphi_i}{\partial q_y} = \frac{\cos \varphi_i}{\|\mathbf{q}_{1:2} - \mathbf{s}_{1:2}^i\|_2}, \quad \frac{\partial \vartheta_i}{\partial q_y} = \frac{s_z^i \sin \varphi_i}{\|\mathbf{q}_{1:2} - \mathbf{s}_{1:2}^i\|_2^2 + (s_z^i)^2}. \tag{51}$$

In addition, the absolute MS position \mathbf{q} is independent of the propagation gain h_i , thus we have

$$\frac{\partial h_i}{\partial \mathbf{q}_{1:2}} = [0, 0]^T. \tag{52}$$

From the above, we complete the derivations of Eqs. (26), (27) and (28) in Section III.

B. Proof of Eqs. (44), (45), (46) and (47)

Take the partial derivative of the (1, 1)th entry of the Fisher information matrix \mathbf{J}_q with respect to ϱ_i as an example.

First, we give the partial derivative of $[\mathbf{J}_q(l)]_{1,1}$ as follows:

$$\begin{aligned}
\frac{\partial [\mathbf{J}_q(l)]_{1,1}}{\partial \varrho_i} &= \frac{\partial \left\{ \frac{2}{\sigma^2} \sum_{m=1}^N \sum_{n=1}^N \Re \left[e^{j(\varrho_n - \varrho_m)} \kappa_{m,n}^{1,1}(l) \right] \right\}}{\partial \varrho_i} \\
&= \frac{\partial \left\{ \frac{1}{\sigma^2} \sum_{m=1}^N \sum_{n=1}^N \left[e^{j(\varrho_n - \varrho_m)} \kappa_{m,n}^{1,1}(l) \right] \right\}}{\partial \varrho_i} \\
&\quad + \frac{\partial \left\{ \frac{1}{\sigma^2} \sum_{m=1}^N \sum_{n=1}^N \left[e^{j(\varrho_m - \varrho_n)} (\kappa_{m,n}^{1,1}(l))^* \right] \right\}}{\partial \varrho_i} \\
&= \frac{1}{\sigma^2} \sum_{m \neq i}^N \left[j e^{j(\varrho_i - \varrho_m)} \kappa_{m,i}^{1,1}(l) \right] \\
&\quad + \frac{1}{\sigma^2} \sum_{n \neq i}^N \left[-j e^{j(\varrho_n - \varrho_i)} \kappa_{i,n}^{1,1}(l) \right] \\
&\quad + \frac{1}{\sigma^2} \sum_{n \neq i}^N \left[j e^{j(\varrho_i - \varrho_n)} (\kappa_{i,n}^{1,1}(l))^* \right] \\
&\quad + \frac{1}{\sigma^2} \sum_{m \neq i}^N \left[-j e^{j(\varrho_m - \varrho_i)} (\kappa_{m,i}^{1,1}(l))^* \right] \\
&= \frac{4}{\sigma^2} \sum_{n \neq i}^N \Re \left[j e^{j(\varrho_i - \varrho_n)} \kappa_{n,i}^{1,1}(l) \right]. \tag{53}
\end{aligned}$$

Then, by using Eq. (39), we obtain that

$$\frac{\partial [\mathbf{J}_q]_{1,1}}{\partial \varrho_i} = \frac{4}{\sigma^2} \sum_{l=1}^L \sum_{n \neq i}^N \Re \left[j e^{j(\varrho_i - \varrho_n)} \kappa_{n,i}^{1,1}(l) \right]. \tag{54}$$

The derivations of Eqs. (45) - (47) follow the similar procedures and here we omit them due to space limitation.

From the above, we complete the derivations of Eqs. (44) - (47) in Section IV.

REFERENCES

- [1] A. Bourdoux, A. N. Barreto, B. van Liempd, C. de Lima, D. Dardari, D. Belot, E.-S. Lohan, G. Seco-Granados, H. Srieddeem, H. Wymeersch, J. Suutala, J. Saloranta, M. Guillaud, M. Isomursu, M. Valkama, M. R. K. Aziz, R. Berkvens, T. Sanguanpuak, T. Svensson, and Y. Miao, "6G white paper on localization and sensing," *arXiv preprint:2006.01779*, June 2020.
- [2] S. Jeong, O. Simeone, A. Haimovich, and J. Kang, "Beamforming design for joint localization and data transmission in distributed antenna system," *IEEE Transactions on Vehicular Technology*, vol. 64, no. 1, pp. 62–76, January 2015.
- [3] A. Shahmansoori, G. E. Garcia, G. Destino, G. Seco-Granados, and H. Wymeersch, "Position and orientation estimation through millimeter-wave MIMO in 5G systems," *IEEE Transactions on Wireless Communications*, vol. 17, no. 3, pp. 1822–1835, March 2018.
- [4] Y. Wang, Y. Wu, and Y. Shen, "Joint spatiotemporal multipath mitigation in large-scale array localization," *IEEE Transactions on Signal Processing*, vol. 67, no. 3, pp. 783–797, February 2019.
- [5] B. Zhou, A. Liu, and V. Lau, "Successive localization and beamforming in 5G mmWave MIMO communication systems," *IEEE Transactions on Signal Processing*, vol. 67, no. 6, pp. 1620–1635, March 2019.
- [6] Y. Liu, E. Liu, and R. Wang, "Energy efficiency analysis of intelligent reflecting surface system with hardware impairments," in *2020 IEEE Global Communications Conference: Wireless Communications (GlobeCom2020 WC)*, Taipei, Taiwan, December 2020.
- [7] Q. Wu and R. Zhang, "Intelligent reflecting surface enhanced wireless network via joint active and passive beamforming," *IEEE Transactions on Wireless Communications*, vol. 18, no. 11, pp. 5394–5409, November 2019.
- [8] Q. Nadeem, A. Kammoun, M. Debbah, and M. Alouini, "3D massive MIMO systems: Modeling and performance analysis," *IEEE Transactions on Wireless Communications*, vol. 14, no. 12, pp. 6926–6939, December 2015.
- [9] S. M. Kay, *Fundamentals of Statistical Signal Processing: Estimation Theory*. Englewood Cliffs, NJ: PTR Prentice-Hall, 1993.
- [10] L. L. Scharf, *Statistical Signal Process: Detection, Estimation, and Time Series Analysis*. Reading, MA: Addison-Wesley, 1991.
- [11] S. L. Collier, "Fisher information for a complex Gaussian random variable: Beamforming applications for wave propagation in a random medium," *IEEE Transactions on Signal Processing*, vol. 53, no. 11, pp. 4236–4248, November 2005.
- [12] X. Zhang, *Matrix analysis and applications*. Cambridge University Press, 2017.
- [13] J. He, H. Wymeersch, T. Sanguanpuak, O. Silven, and M. Juntti, "Adaptive beamforming design for mmwave RIS-aided joint localization and communication," in *2020 IEEE Wireless Communications and Networking Conference Workshops (WCNCW)*, 2020, pp. 1–6.